Institute of Paper Science and Technology
Atlanta, Georgia

IPST TECHNICAL PAPER SERIES

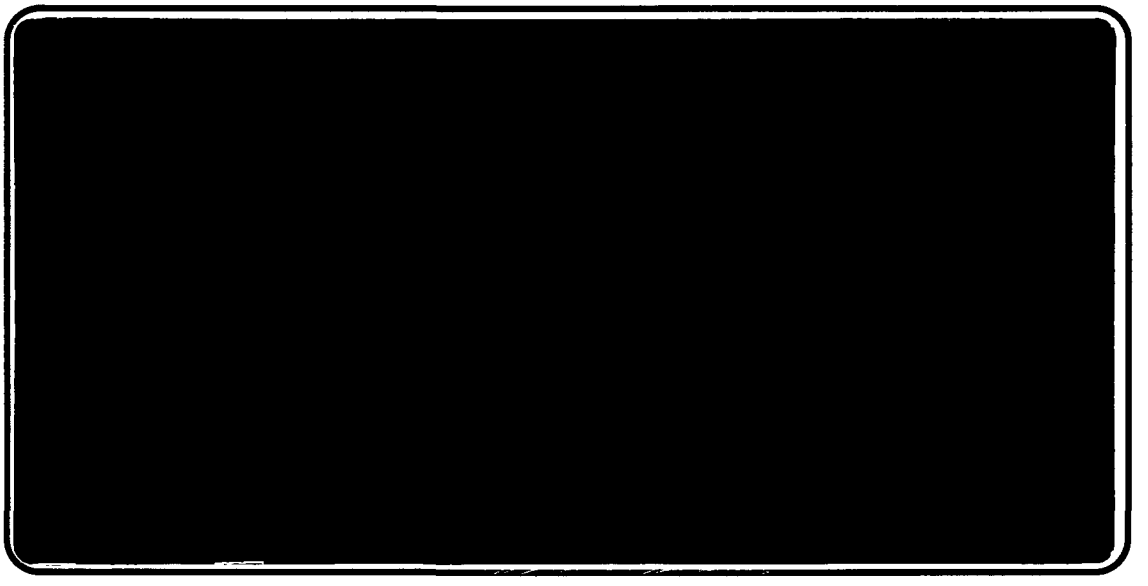

NUMBER 388

FLOW VISUALIZATION OF AIR ENTRAINMENT AND DYNAMIC CONTACT LINE INSTABILITY IN LOW-SPEED ROLL COATING

P.J. VEVERKA AND C.K. AIDUN

AUGUST, 1991

Flow Visualization of Air Entrainment and Dynamic Contact Line Instability in Low-Speed Roll Coating

P.J. Veverka and C.K. Aidun

To be presented at
1991 TAPPI Engineering Conference
Nashville, Tennessee
September, 1991

FLOW VISUALIZATION OF AIR ENTRAINMENT AND DYNAMIC CONTACT LINE INSTABILITY IN LOW-SPEED ROLL COATING

Peter J. Veverka
Graduate Student

Cyrus K. Aidun
Assistant Professor

Engineering Division
The Institute of Paper Science and Technology
575 14th Street N.W.
Atlanta, GA 30318 USA

ABSTRACT

Almost all surface application systems, such as coating or sizing processes, involve displacement of air by liquid at a common interfacial line known as wetting or dynamic contact line. The fact that the contact line destabilizes and air entrainment occurs beyond a critical wetting speed is well known (1-12). In contrast to other studies which focus primarily on measuring the air entrainment speed , we use flow visualization to observe the sequence of events leading to air entrainment. By employing high-speed cinematography along with the proper lighting arrangement that exploits differences in the refractive index at phase boundaries, a visualization technique was found. The importance of air entrainment speed limitations is emphasized and elucidation of the events surrounding this defect can lead to better design of thin-film application equipment. Two mechanisms are presented at speeds just above the critical velocity. Our flow visualization studies support Scriven's (13) proposed mechanism hypothesizing the air film collapse.

KEYWORDS

Air entrainment, dynamic contact line, flow visualization, total internal reflectance, refractive index, high-speed photography, illumination, Newtonian fluids, glycerol

INTRODUCTION

Visual evidence is one of the most satisfactory ways of resolving doubts and gaining both qualitative and quantitative information. A method for observing the desired area must first be designed with the proper magnification, illumination and contrast. Direct observation with the coating colors for paper and board application is difficult because they are generally opaque. They do not readily allow for flow visualization without special techniques, e.g., flash X-ray. Therefore, a more fundamental study was conducted with glycerin, a transparent, Newtonian liquid. The dynamic contact line (DCL) was formed with a rotating roll in a clear Plexiglas™ tank. The DCL is a three-phase intersection,

where two or more of the phases are in motion in the Eulerian sense. The DCL problem is not particular to the paper industry, and some of the most well-known

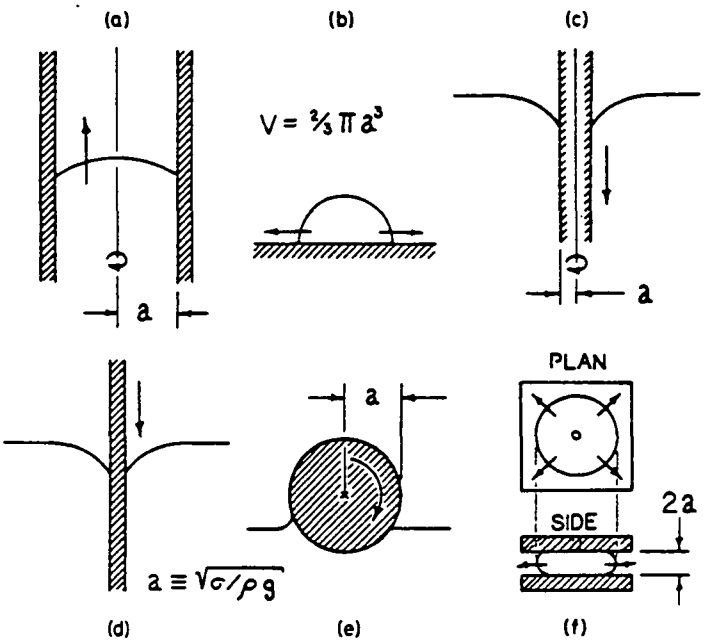

Figure 1. (a) The mutual displacement of two immiscible fluids through a capillary of radius 'a'. (b) The spreading of a drop of liquid volume V on a flat surface. (c) The submerging of a cylinder of radius 'a' into a bath of liquid. (d) The submerging of a tape into a bath of liquid. (e) The rotation of a cylinder of radius 'a' partially submerged into a bath of liquid. (f) The spreading of a liquid between two parallel plates in which the liquid is introduced through a hole in the center of the top plate. From reference (20).

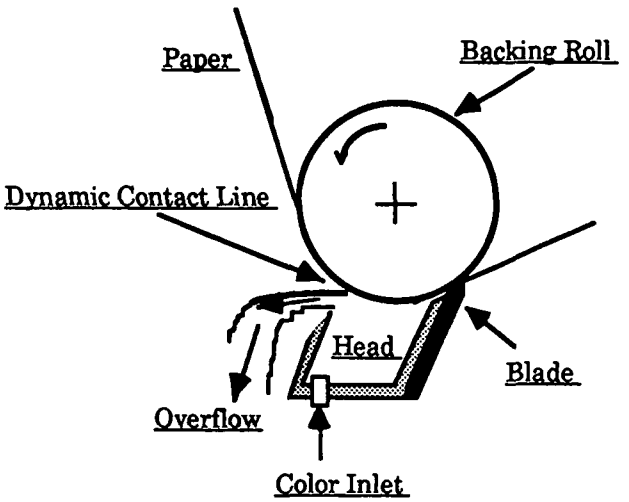

Figure 2 . Short-dwell coating head with location of DCL at intersection of paper, color, air interface. The size of the coating head has been enlarged to show details of DCL.

configurations are shown in Figure 1. Figure 1(d) could be thought of as paper entering the pond on a horizontal squeeze roll size press, while the configuration we studied in Figure 1(e) is analogous to the backing roll in a short-dwell coater. The location of the DCL shown in Figure 2 with a short-dwell head reemphasizes the difficulty in conducting flow visualization studies with full-scale equipment. Previous investigators (1-12) have noted that the DCL on a macro scale passes from a straight line into a jagged or "sawtooth" configuration above a critical velocity. It is the instability of the DCL in the sawtooth configuration that leads to air becoming entrained. The critical air entrainment velocity is mainly influenced by the viscosity of the fluid phase. The DCL in the short-dwell head is assumed to form the same sawtooth configuration but has not been visually recorded. Industry is particularly concerned with air entrainment because it leads to differential processing effects, i.e.,"skipping" and impairs the overall efficiency of the operation (2,13,16,17). No experimentation to our knowledge has visually captured the events leading up to and including air entrainment itself with either clear, Newtonian fluids or opaque coatings. Quantitative results from (1-12) and industrial research coupled with insight into a mechanism of air entrainment could lead to a breakthrough in designing the next generation of ultrahigh-speed application equipment.

Here, we review some relevant and basic principles of light refraction and also high-speed cinematography. The procedure used in the experimentation will then be presented followed by experimental observations. Finally, a discussion and conclusion section will summarize the mechanisms of air entrainment that we have found.

Basics on Light and Refraction

The technique used in visualizing air entrainment involve some basic principles of light refraction. Light could be viewed as a wave that obeys the universal principle of wave propagation. For simplification of the discussion, the ray theory of light will be approximated. The ray theory is applicable when the size of the light beam and the obstacles it interacts with are much greater than the wavelength of light (15). When a beam of light passes from one medium to another, and the speed of light is different in the second medium, the light beam is refracted, that is, the wavefronts are uniquely spaced dependent on the speed of light in the material. Fermat's principle of least time states that when a beam of light passes into a material with a different refractive index, it will follow the path requiring the shortest traveling time.

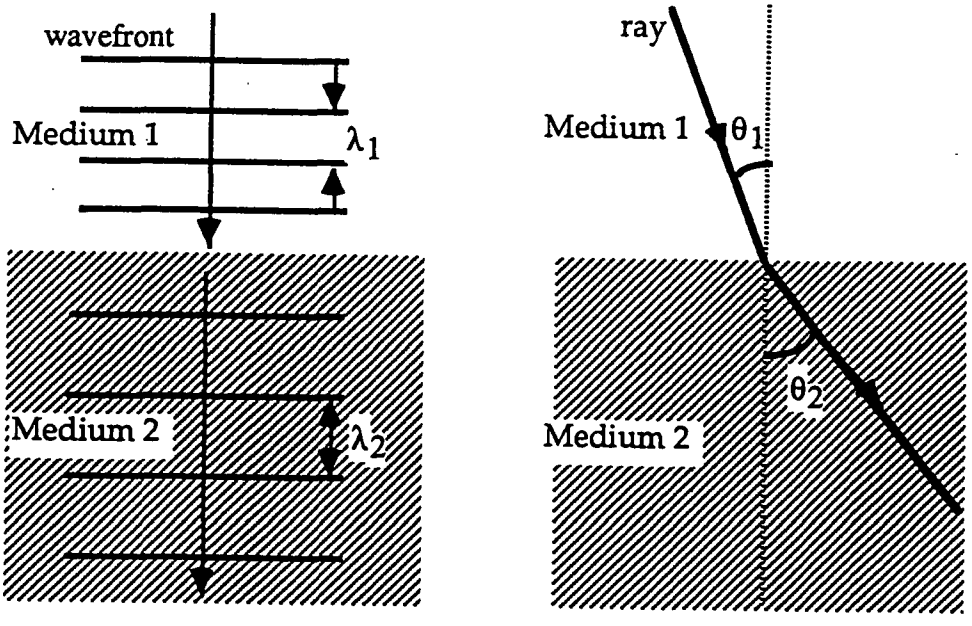

Figure 3. Illustrates refraction, due to light passing through different media. Index of refraction in medium 2 < medium 1.

These two physical laws are shown in Figure 3. The absolute refractive index, n_a, is defined as the ratio of the speed of light in a vacuum, c, over the speed of light in the medium v_i and is given by

$$n_a \equiv \frac{\sin\theta}{\sin\theta_i} = \frac{c}{v_i} \qquad (1)$$

where θ and θ_i are the corresponding vacuum and medium ray angles with respect to the normal. The relative index of refraction, n, is the ratio of the two absolute indices of refraction, n_1 and n_2, given by

$$n = \frac{\sin\theta_1}{\sin\theta_2} = \frac{n_2}{n_1} \qquad (2)$$

A limiting case where $\theta_2 = 90°$, and thus $\sin\theta_2 = 1$, is known as total internal reflectance and can be employed to form image outlines at the transition between materials. Total internal reflection can occur when a beam travels from a high refractive index to a lower index, which is the same as saying that the velocity in the second material is greater than the first. The angle of incidence at which this occurs is known as the critical angle of incidence, θ_c, and for any angle $\theta > \theta_c$, total internal reflection develops. This critical angle, θ_c, can be calculated by

$$(n_1 > n_2),\ \sin\theta_c = \frac{n_2}{n_1} \qquad (3)$$

or determined through trial and error by slowly changing the angle of incidence until a darker area of total reflection results. The principle of total internal reflection can be exploited in multiphase systems at phase boundaries, providing that the light beam travels from a high to low refractive index phase. Simple adjustment of lighting will give optimum contrast at phase boundaries. The re-

fractive index for glycerin, Plexiglas™(methyl methacrylate) and air are given in Table I.

Table I

	Absolute index, n	Notes
Air (STP)	1.003	
Glycerin	1.47- 1.45	100-88 Wt%
Plexiglas™	1.49	

Background on High-Speed Cinematograhy

In our studies, we have used a HYCAM®, which is a high-speed 16 mm camera designed for the acquisition of photographic data pertaining to high-speed or short-lived events. It uses the rotary prism and continuous film flow principles of operation and is capable of filming up to 11,000 frames per second (fps) with a full-frame optical head through 44,000 fps with a quarter-frame head. The HYCAM is limited by its geometric aperture of f/3.2. A built-in crystal generator known as the timing light generator (TLG) driven at selectable frequencies of 100, 1000 and 5000 Hz marks the inboard film edge. The TLG signal has an accuracy of 0.01% and, thus, provides high precision in determining elapsed time between events. Standard video and high shutter speed video (both 30 fps) were used unsuccessfully because of insufficient resolution and speed, although their immediate review of experimental data is a definite advantage. The definition usually adopted for high-speed photography is pictures taken at an exposure time of less than 1000 microseconds or at a repetition rate greater than 250 pictures per second(18). The cost/benefit ratio and long-term usage requirements between electronic and mechanical high-speed systems must judiciously be considered before committing to any one system. An excellent review article by Sweatt et al. (19) compares state-of-the-art mechanical and electronic systems.

A high level of illumination is required with high-speed photography, and foot-candle requirements increase rapidly as filming speeds increase. The tungsten-halogen lamp is one of the most common incandescent lamps for diffuse lighting in photography. The input energy is converted to visible light with a color temperature of 3600 K ; however, 80% of the input energy is transformed into heat (IR) at the lamp (14). If concentrated light is required for a small area, the tungsten-halogen lamp may melt or damage the experiment if not protected in this situation.

PROCEDURE

As mentioned earlier, proper magnification, illumination and contrast are required to obtain good results. It was decided that the best setup would include using a mirror and a Kiron f/4.5 70-210 mm zoom lens which allowed for filming approximately 6' away from the subject. Distance markers were made on the roll's surface to determine sawtooth dimensions and to calculate the accurate linear roll speed from the TLG marks on the film. Four 1000W tungsten-halogen lamps were positioned directly over the experimental apparatus behind a white

linen diffuser shade. The diffuser shade helped to eliminate glare. Figure 4 presents the details of the experimental setup used in the visualization. Sufficient light was available for filming at 240 fps and an aperture of f/4.5 when using Eastman Kodak 4-X Reversal 16 mm (400 ASA, B&W, 7277) film. Color film is also available but has a slightly lower resolution. Upon viewing developed films, it was felt that the framing rate provided good detail between events, although higher roll velocities would require faster framing rates and thus more light. The maximum linear roll speed is 26.7 m/min.

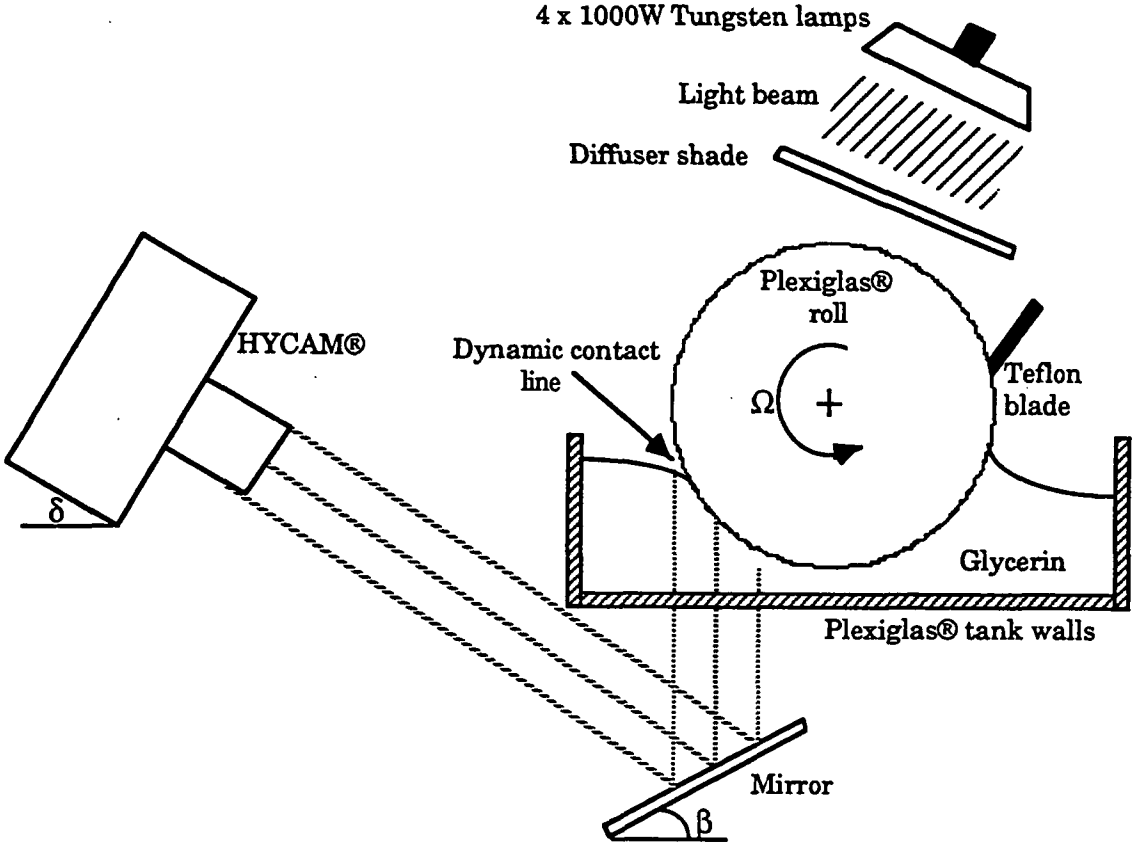

Figure 4. Experimental setup used for flow visualization.

The laws of refraction mentioned in the previous section provided excellent contrast between phases. Total internal refraction occurred at the Plexiglas™/air interface within an air pocket of the sawtooth configuration. Wherever air entrainment was occurring, a dark area appeared in the positive final print with the reversal process. The transfer to video was made on a Rank Cintel machine via digital tape to super VHS. The video is a negative of the positive 16 mm film. A significant advantage of this dubbing process is that a frame-by-frame time code can be electronically "etched" onto the video image allowing for accurate identification of a particular segment of the film. The video signal is sent to an image analyzer for quickly measuring the dimension on a single frame.

OBSERVATIONS

The photo series in this presentation is not as clear as direct observation of the films or video shown in slow motion. The photos in Figure 5, are 35 mm positive reproductions of the 16 mm frames presented in time sequence and show the collapse of an air pocket toward the left side of each frame. The distance markers on the roll surface are 1 cm apart and the cross-hair dimensions can be inferred from these. Successive viewing and reviewing of the videotapes illuminated some possible mechanisms under which air entrainment was occurring. The fast frame rate, on the fringe of high-speed photography, coupled with the proper lighting arrangement, gave excellent contrast and detail.

DISCUSSION AND CONCLUSIONS

The objective in this study is to gain insight into air entrainment in coating systems by using a simple configuration. Application of the high-speed camera and lighting arrangements is possible only in systems that allow for light to penetrate. Let us suppose that a SDTA (short-dwell time applicator) is available that allows us to see through the coating head at industrial speeds. We will also assume that the air entrainment rate is proportional to the linear speed and that lighting requirements are also directly proportional for the same exposure. This is only an approximation, and actual requirements may be higher. If the SDTA entrains air at 1500 m/min, which is ≈60 times faster than our highest experimental speed (26.7 m/min), we would require about 240 kW of illumination to film at 14,400 fps with direct illumination. High-speed strobes and pulsed laser sources would need to be examined as opposed to direct illumination for fear of melting the equipment.

Mechanisms of Air Entrainment

Over 24,000 frames of film were taken and viewed to determine if some sort of mechanism or series of events caused the air pocket to break up and entrain air with the simple apparatus used. Two distinct and separate mechanisms (M1 and M2) have been observed to varying degrees in the collected films. These will be described and then illustrated with photos taken from the 16 mm film. Only certain quadrants of the pictures are meant to illustrate a specific case of initiation, propagation, entrainment and reemergence of a particular flow structure. If the photo is divided vertically by the cross hairs on the picture, the middle two quadrants from line to line are each 16.3 mm wide. This gives an idea of the structure dimensions.

M1 (not shown in photos) begins with the air pocket growing to a critical size and a liquid "bridge" penetrating the air pocket in the main body of the air pocket as displayed in Figure 6. The main body is defined as on or near the geometric center of the triangular-shaped air pocket. The bridge then grows radially outward displacing air until it meets the air liquid boundary at the edge of the triangular air pocket. This produces a trapped gas area at the former tip of the

triangular air pocket, which coalesces into a bubble and is carried by the bulk flow of the fluid as gaseous air.

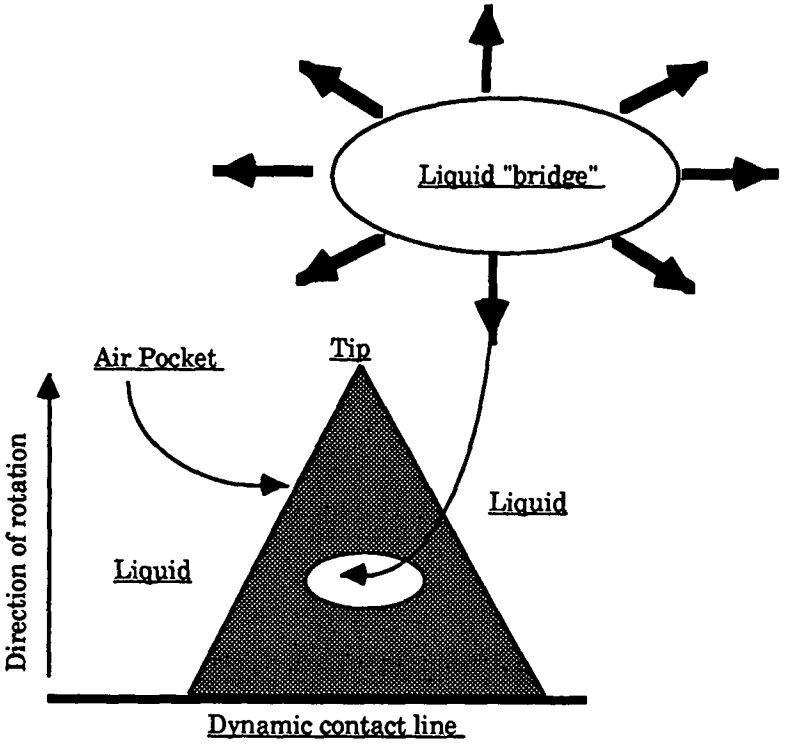

Figure 6. The mechanism of radial outward growth of a liquid bridge in the air pocket. The arrows on the bridge represent the direction of advance.

M2 starts at the base edges of the air pocket as liquid bridges, growing radially inward toward the center of the air pocket. Once the advancing liquid fronts meet, the air pocket above is effectively isolated and thus can enter only into the liquid. M2 is displayed in Figure 5 of this paper. Frame #1 is meant to illustrate the sawtooth structure before air entrainment. Frames #43-51, on the left side of each photo, show the bridging by the liquid at the edges of the air pocket. Total internal reflection ceases where the glycerin has bridged through the air pocket because it has a unique critical angle of refraction. In Frames #53-55 the air pocket at the tip is isolated and can only be entrained as a bubble into the liquid shown in Frames #56, 58 and 81. Frames #141, 201 and 241 show the reemergence of the sawtooth structure that eventually will entrain air again. Calculation of the approximate air pocket film thickness from bubble diameter indicates that it is on the order of 5-20 μm which agrees with predictions made by Scriven (13).

Mechanical photography proved to be a good method of conducting this experiment in the laboratory and allowed for identification of two mechanisms of air entrainment that support Scriven's (13) hypotheses.

LITERATURE CITED

1. B.S. Kennedy and R. Burley, J. Colloid Interface Sci., "Dynamic Fluid Interface Displacement and Prediction of Air Entrainment," 62(1):48-62 (1977).

2. R. Burley and B.S. Kennedy, Chem. Eng. Sci., "An Experimental Study of Air Entrainment at a Solid/Liquid/Gas Interface," 31:901-11 (1976).

3. B. Bolton and S. Middleman, Chem. Eng. Sci., "Air Entrainment in a Roll Coating System," 35:597-601 (1976).

4. T.D. Blake and K.J. Ruchak, Nature, "A Maximum Speed of Wetting," 282: 489-491 (1979).

5. R. Burley and R.P.S. Jolly, Chem. Eng. Sci., "Entrainment of Air into Liquids by a High Speed Continuous Solid Surface," 39: 1357-1372 (1984).

6. T.M. Sullivan and S. Middleman, Chem. Eng. Commun., "Roll Coating in the Presence of a Fixed Constraining Boundary," 3:469-482 (1979).

7. W.L. Wilkinson, Chem. Eng. Sci., "Entrainment of Air by a Solid Surface Entering a Liquid/Air Interface," 30:1227-30 (1975).

8. E.B. Guttoff and C.E. Kendrick, AIChE Journal, "Dynamic Contact Angles," 28(3): 459-466 (1982).

9. R.T. Perry, Ph.D. Thesis, Univ. of Minnesota, U.S.A., 1967.

10. M.T Ghannam and M.N. Esmail, AIChE Journal, "Effect of Substrate Entry Angle on Air Entrainment in Liquid Coating," 36(8): 1283-1285 (1990).

11. M.T Ghannam and M.N. Esmail, Canadian Journal of Chemical Engineering, "Air Entrainment and Dynamic Contact Angles in Hydrodynamics of Liquid Coating, " 68:197-203 (1990).

12. R.A. Buononpane , E.B. Gutoff, and M.M.T. Rimore, AIChE Journal, "Effect of Plunging Tape Surface Properties on Air Entrainment Velocity," 32(4): 682-683 (1986).

13. L.E. Scriven, 1982 AIChE Winter Meeting, "How Does Air Entrain at Wetting Lines," Unpublished presentation at Symposium of Coating Operations, Orlando, Florida.

14. P. Kiankhooy, "HMI Lighting for High Speed Applications," High Speed Photography, Videography and Photonics VI, Gary L. Stradling, Editor, Proc. SPEI 981, p.231-241, (1989).

15. N.P. Cheremisnoff, Instrumentation for Complex Fluid Flows, 1'st ed., Technomic Publishing Company, Inc., Lancaster, PA, 1986, p.111-117.

16. M.J. Ducey, Pulp and Paper, "New short-dwell coaters reduce raw material losses and downtime," 58(6):102-104 (1984).

17. H. Sommer, "Applicating Systems for Coating ULWC and MFP Papers" in 1988 TAPPI Coating Conference Proceedings, TAPPI Press, Atlanta, 1988, p. 131-137.

18. W.D. Chesterman, "World Progress in High Speed Photography from 1935 to 1953" in Science and Applications of Photography - Proceedings of the R.P.S. Centenary Conference London 1953, The Royal Photographic Society of Great Britain, London, 1955, p.356.

19. W.C. Sweatt ,G.S. Phipps, R.N. Shagam, and R.A. Hill, "Comparison of mechanical and electronic high speed recording systems," High Speed Photography , Videography and Photonics VI ,Gary L. Stradling, Editor, Proc. SPEI 981, p.306-315 (1989).

20. Dussan, E.B., Ann. Rev. Fluid Mech.,"On the Spreading of Liquids on Solid Surfaces : Static and Dynamic Contact Lines," 17: 54-89 (1979).

ACKNOWLEDGEMENTS

This research was supported in part by an industrial consortium through the Institute of Paper Science and Technology. Portions of this work were used by P.J.V. as partial fulfillment of requirements for the M.S. degree at the Institute of Paper Science and Technology.

Figure 5 - Photo Series (249.6 cp, 15.55 m/min)

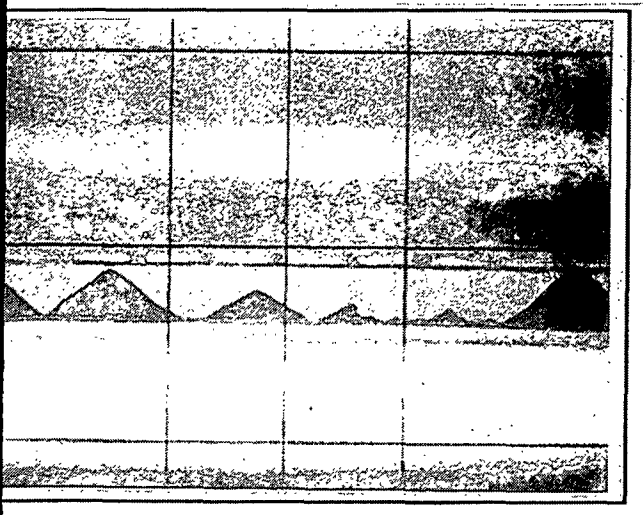

Frame #1, 0 ms elapsed

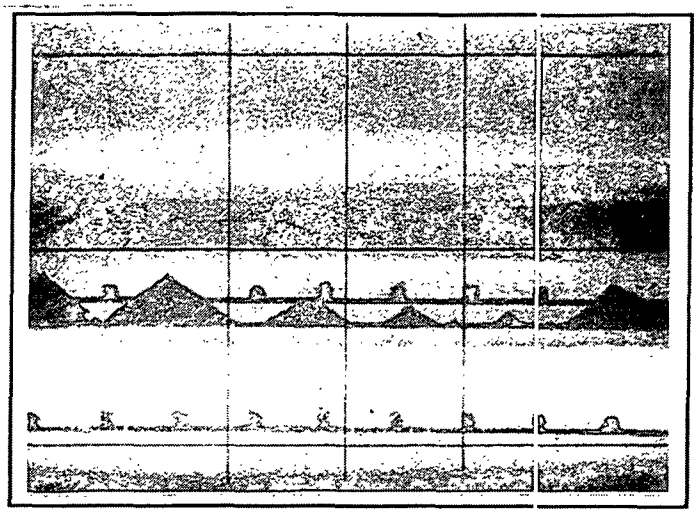

Frame #43, 162.5 ms elapsed

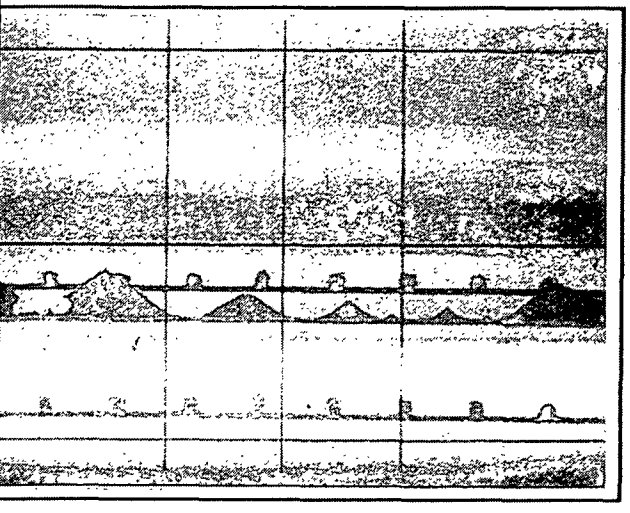

Frame #45, 170 ms elapsed

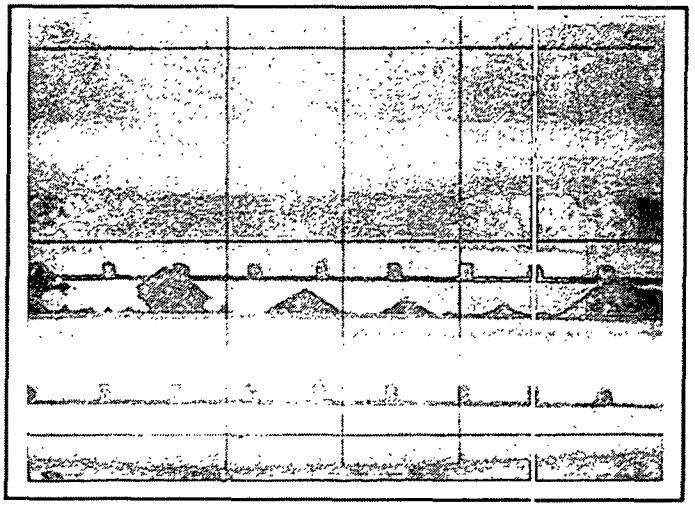

Frame #47, 178 ms elapsed

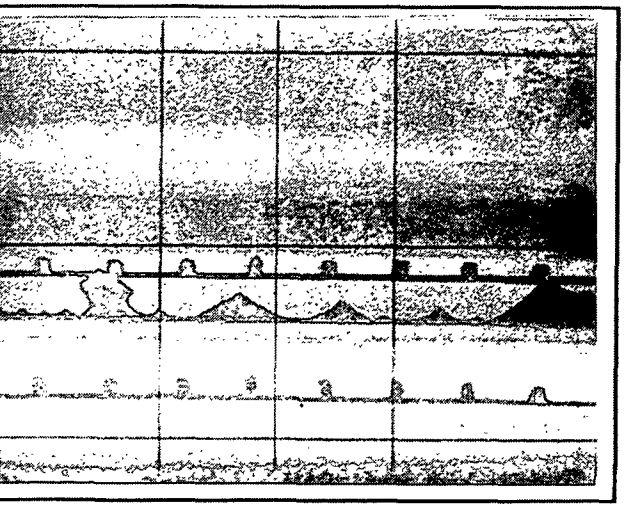

Frame #49, 186 ms elapsed

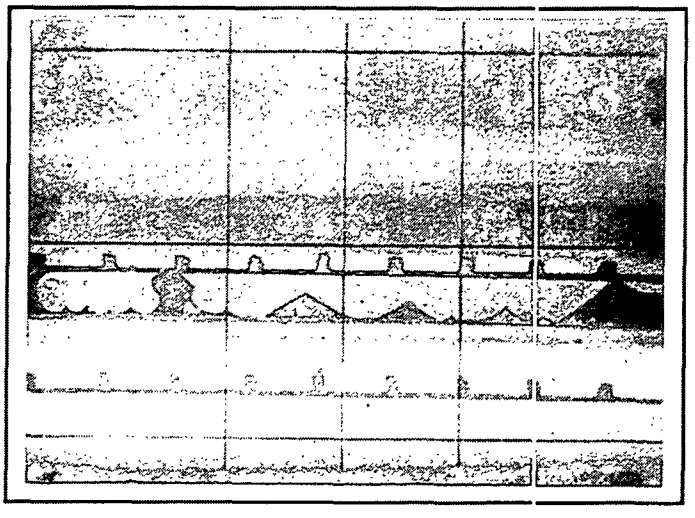

Frame #50, 190 ms elapsed

Figure 5 - Photo Series (249.6 cp, 15.55 m/min)

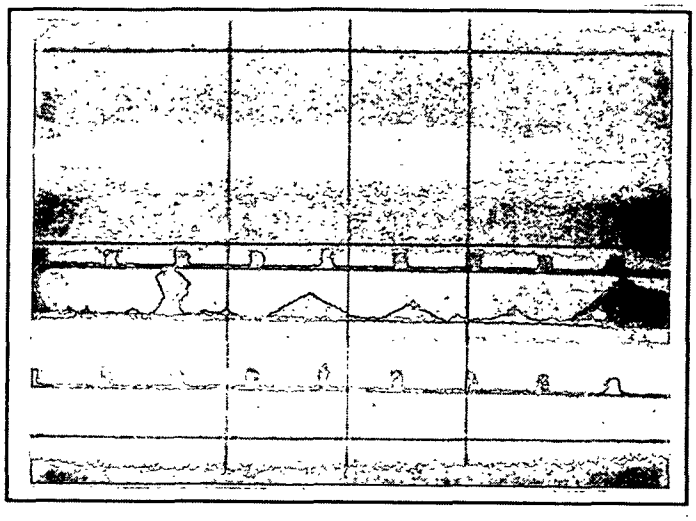

Frame #51, 194 ms elapsed

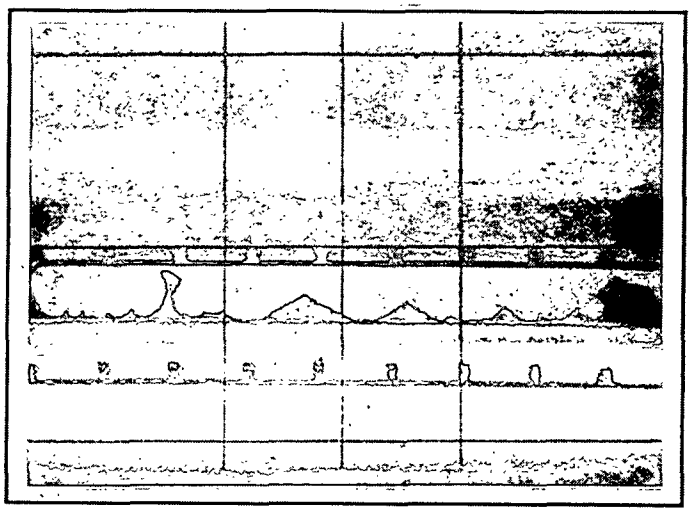

Frame #53, 201 ms elapsed

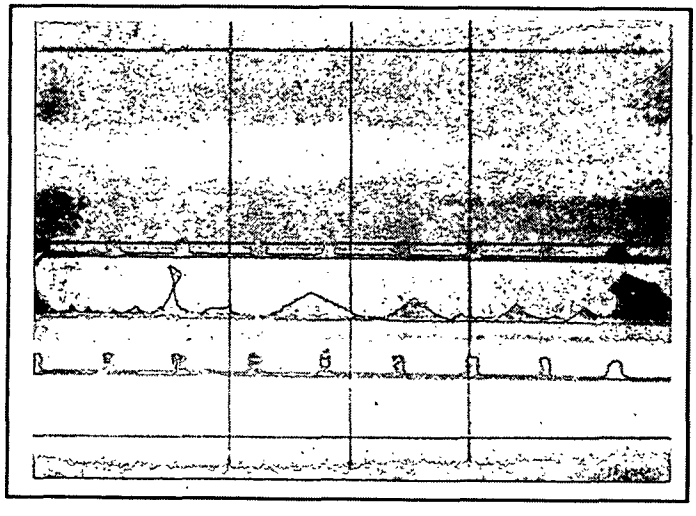

Frame #54, 205 ms elapsed

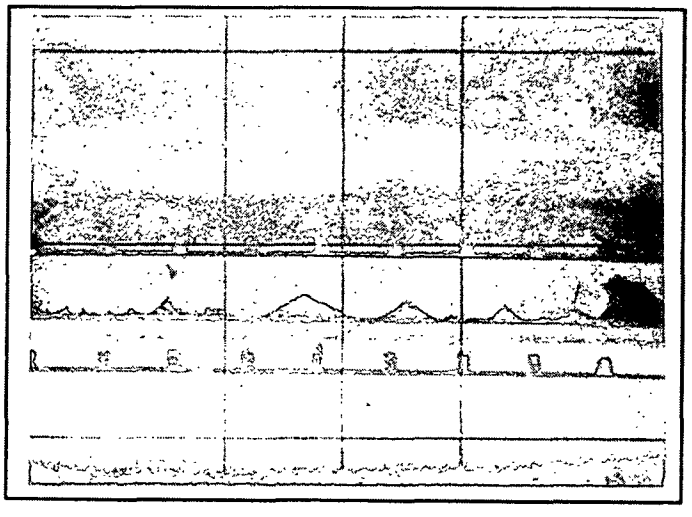

Frame #55, 209 ms elapsed

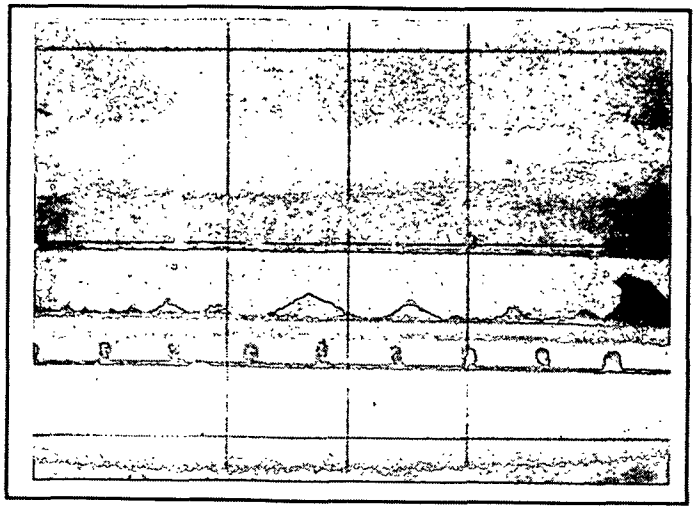

Frame #56, 213 ms elapsed

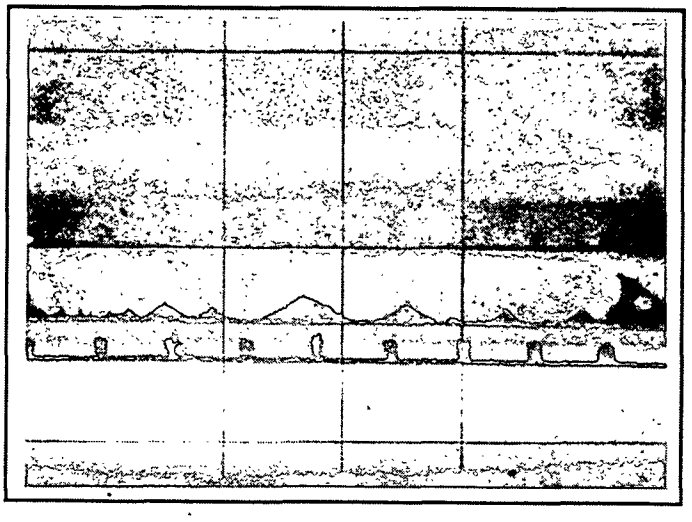

Frame #58, 221 ms elapsed

Figure 5 - Photo Series (249.6 cp, 15.55 m/min)

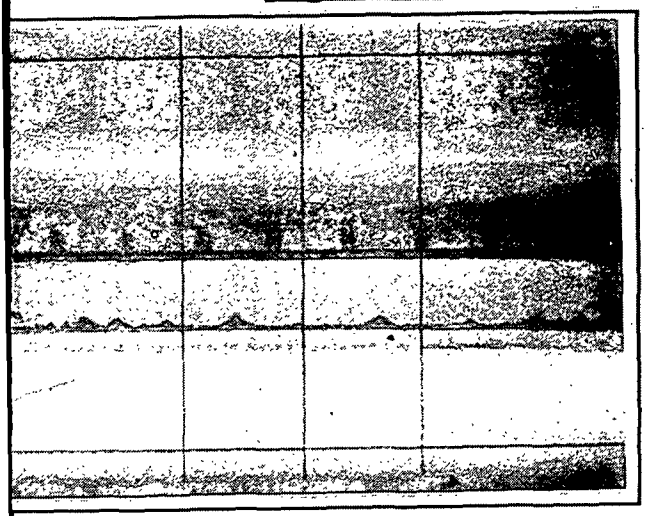

Frame #81, 304 ms elapsed

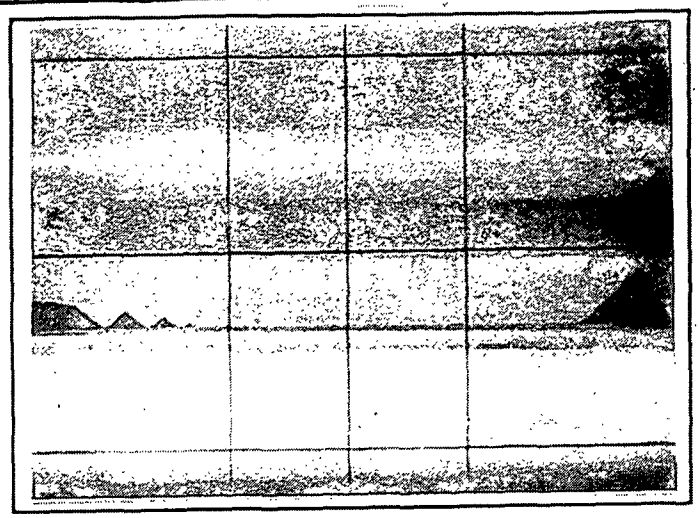

Frame #141, 542 ms elapsed

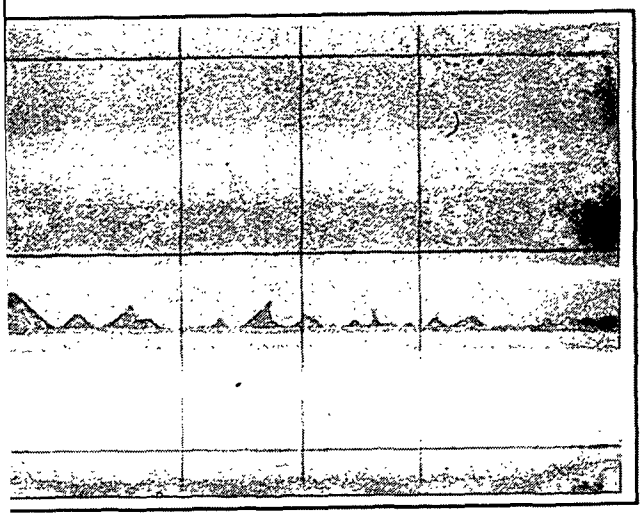

Frame #201, 774 ms elapsed

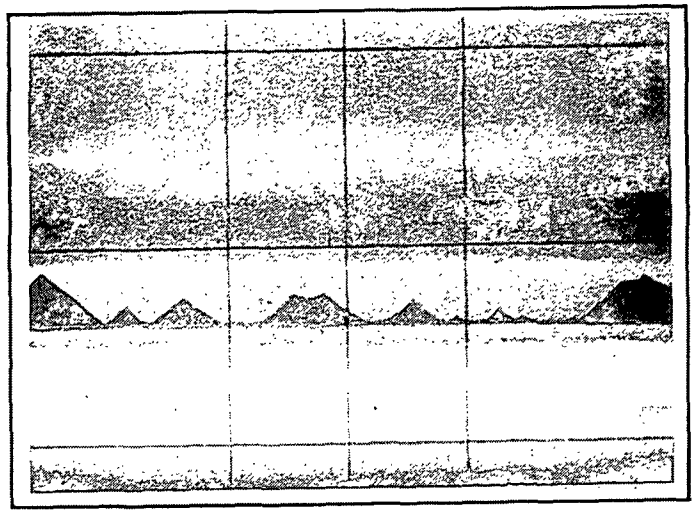

Frame #241, 923 ms elapsed